Radiation From 3D Sources in the Presence of 2D Composite Objects of Arbitrary Cross-Sectional Shape

Ahmed A. Kishk[1], Peter Slättman[2] and Per-Simon Kildal[3]
[1] Department of Electrical Engineering, University of Mississippi
University, MS 38677, USA
[2] Smartwaves International
3385 Scott Boulevard, Santa Clara, CA 95054, USA
[3] Electromagnetics Department, Chalmers University of Technology
S-412 96 Göteborg, SWEDEN

Abstract

A method of moment code for computing the radiation from arbitrarily oriented narrow slots or straight dipoles in the vicinity of a two dimensional (2D) multi-region composite cylinder of arbitrary cross-sectional shape and infinite extension in the z-direction is developed. The dipoles and the slots are represented by known equivalent electric and magnetic currents distributions, respectively. The finite extent of the sources are included by Fourier transforming the equivalent electric and magnetic source currents along the infinite cylinder axis. The computed radiation patterns are compared to results computed by other methods and measurements. Radiation patterns are predicted both in the elevation and azimuthal planes.

1 Introduction

Antennas consisting of three-dimensional (3D) radiating elements (sources) and two-dimensional (2D) structures (cylinders of infinite extent) can be analyzed by using a spectrum of two-dimensional solutions (S2DS), as described in [1]. Such antennas are for instance dipoles at long and narrow ground planes, or slots cut in a cylindrical surface. Generally, any antenna consisting of slots or dipoles in or in the vicinity of 2D structures of arbitrary cross-sectional shape and material combination can be analyzed by the S2DS technique. The purpose of the present paper is to present the formulation and some selected results for this general case.

The most significant part of an S2DS analysis is to solve repeatedly the special spectral domain problem obtained by Fourier-transforming the sources in the z-direction of the structure. This spectral domain problem can be interpreted as a harmonic 2D spatial problem where the sources (and the resulting fields) have harmonic z-variation of the form $e^{-jk_z z}$ where $k_z = 0$ corresponds to the standard 2D problem. This general harmonic 2D problem must be solved for a large number of values of the spectral variable k_z in order to inverse transform to 3D spatial domain. The radiation pattern, however, can normally be found directly from the 2D harmonic solution without inverse transformation.

The harmonic 2D problem is conveniently solved for each k_z by the method of moment (MoM). Several approaches have previously been used; the field within baffles has been expanded in parallel-plate modes and solved by MoM [2], the field within a virtual circular cylinder around a triangular mast has been expanded in cylindrical sector waveguide modes and solved by MoM [3], and the induced currents on a 2D metal structure with arbitrary cross-sectional shape have been solved by MoM [4] with a decoupled electric field integral equation (EFIE) [5].

In two previous papers plane wave scattering from two-dimensional composite objects [6], and scattering from an impedance cylinder with arbitrary cross-section under oblique plane wave incidence were analyzed [7], where the equivalent electric and magnetic currents were solved for by pulse expansion and point-matching. The present paper extends that work by including equivalent electric and magnetic sources in order to model slots and dipoles in a two-dimensional structure with multiple regions of perfect electric conductors (PEC's) and homogeneous and isotropic materials. The pertaining integral equations are presented and a computer code is developed.

The computer code is verified against examples from the literature, measurements, analytic solutions and a code for coaxial multi-layer circular cylinders.

2 Statement of the Problem

We assume that we have a composite 2D object parallel to the z-axis and that 3D sources are present in its neighborhood such as dipoles, or attached to it such as slots or printed microstrip dipoles. It is very time consuming to solve the radiation problem in its present form in the spatial domain. Instead the problem will be solved in the spectral domain as a spectrum of 2D solutions as will be shown in Section 3. We will assume that the equivalent current distributions of the 3D sources are known. As in most practical applications of thin sources such as dipoles or narrow slots, the equivalent electric and magnetic current distributions, J and M can be assumed sinusoidal of the form

$$\mathbf{J}(u,v) = \frac{1}{W}\sin(\frac{\pi}{L}(u-\frac{L}{2}))\delta(v)\hat{\mathbf{u}}_s, \quad -L/2 \le u \le L/2 \tag{1}$$

where W is an equivalent width of the source and L is the length. The equivalent width is much smaller than both L and the wavelength. The variables u and v are the local coordinates of the source and $\hat{\mathbf{u}}_s$ is the unit vector along the current source. After transforming the source coordinates to the cylindrical coordinates (ρ, z) and using the Fourier transform defined by

$$\tilde{\mathbf{J}}(\rho, k_z) = \int_{-\infty}^{\infty} \mathbf{J}(\rho, z)e^{jk_z z}dz \tag{2}$$

and the inverse Fourier transform as

$$\mathbf{J}(\rho, z) = \frac{1}{2\pi}\int_{-\infty}^{\infty} \tilde{\mathbf{J}}(\rho, k_z)e^{-jk_z z}dk_z \tag{3}$$

where k_z is the axial wavenumber. The Fourier transform of the current in (2) with respect to z is

$$\tilde{\mathbf{J}}(t, k_z) = \begin{cases} \frac{1}{W\cos\alpha}\sin(\frac{\pi}{L}(\frac{t}{\cos\alpha}-\frac{L}{2}))e^{jk_z t\tan\alpha}, & \text{if } \alpha \neq 90° \\ -\frac{2\pi L}{W(\pi^2-k_z^2L^2)}\cos(k_zL/2)\delta(t) & \text{if } \alpha = 90° \end{cases} \tag{4}$$

$$|t| \le \frac{L}{2}\cos\alpha$$

where α is the angle between the source axis u and the xy-plane, and t is the projection of u in the xy-plane. The Fourier transformed current source written as $\tilde{\mathbf{J}}(t, k_z)e^{-jk_z z}$ for a particular value of k_z located in the presence of the infinitely long 2D structure, can be visualized as an infinite current sheet of width equal to the projected length of the current in the xy-plane and parallel to the z-axis with harmonic variations in the z-direction [1].

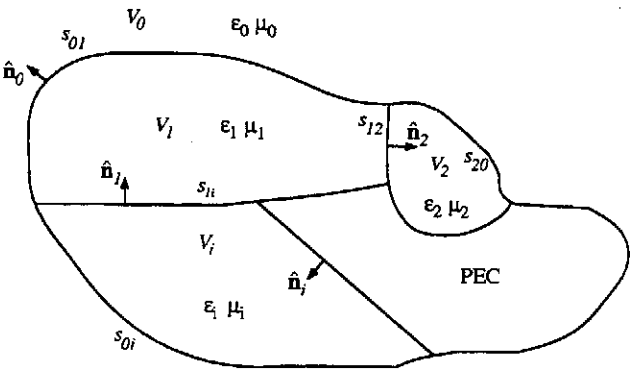

Figure 1: Cross-section of a general cylinder.

Therefore, the total fields produced by these harmonic 2D sources must be harmonic in z as well in order to satisfy the boundary conditions on the objects [1]. For each value of k_z, the problem can be considered a two dimensional problem which should be solved an infinite number of times to cover all of the k_z spectrum, and which will be summed to get the solution in the spatial domain. This process is not necessary if the primary interest is the farfield radiation patterns. For each value of $k_z \in [-k, k]$, the farfield is radiating on a cone around the z-axis with cone angle $\theta = \arccos(k_z/k)$, where k is the wave number in free space. Thus, the farfield can be computed directly from the spectral domain solution, i.e. the 2D solution [1].

In this paper, the time variation $e^{j\omega t}$ is implied and suppressed throughout.

3 Formulation of the 2D Problem

Now that we have shown that the 3D sources can be transformed to harmonic 2D sources in the spectral domain and have transformed the whole problem to a spectrum of 2D problems, let us describe the general arbitrary shape of the 2D object and derive the integral equations. The geometry and notations of such an object are given in Fig. 1. The whole space is divided into N+1 homogeneous regions, V_i, which may be either dielectric regions with permittivities ϵ_i and permeabilities μ_i, or closed conductor regions. These regions are numbered $i = 0, 1, 2, ..., N$, where $i = 0$ corresponds to the exterior region, i.e. free space. Lossy materials are considered by allowing ϵ_i and μ_i, $i = 1, 2, ..., N$ to be complex. Each region V_i is surrounded by a closed surface S_i and associated with an inward directed normal unit vector $\hat{\mathbf{n}}_i$. The surface interface between regions V_i and V_j is

denoted as $S_{ij}, i \neq j$. Thus, S_i comprises the set of all interface surfaces S_{ij}, where j represents all region numbers adjacent to region V_i. Note that S_{ij} is the same surface as S_{ji}; however, the normal unit vectors $\hat{\mathbf{n}}_i$ and $\hat{\mathbf{n}}_j$ are in opposite directions to each other on the two surfaces. The concept of the equivalence principle is used to derive a surface integral equation (SIE) formulation for 2D objects with $N+1$ homogeneous regions. The total fields in each homogeneous region are denoted by $\mathbf{E}^i$ and $\mathbf{H}^i$, $i = 0, 1, 2, ..., N$ for the electric and magnetic fields, respectively. Any perfectly conducting region need not be considered as a region because the fields are known to be equal to zero. In the free-space region V_0, the total fields are denoted by $(\mathbf{E}^0, \mathbf{H}^0)$. In this paper, the excitations are considered to be 3D equivalent electric or magnetic current sources with known amplitudes and current distributions. The electric sources are arbitrarily located inside any number of regions to model thin wire radiators or on the dielectric surface interfaces to model printed sources. Slots are modeled by magnetic sources on the conducting surfaces. From Maxwell's equations and the equivalence principle, one can express the fields in each region in terms of unknown electric and magnetic equivalent surface currents plus the fields due to the harmonic 2D sources present in the region.

According to the surface equivalence principle we can break the original problem into a number of auxiliary problems that are equal to the number of nonperfect conducting regions. To obtain the ith auxiliary problem the boundaries of region V_i are replaced by equivalent surface currents radiating in a homogeneous medium with the constitutive parameters of region V_i using electric currents for the conductor boundaries and equivalent electric and magnetic currents for the dielectric boundaries. The electric and magnetic currents appearing on opposite sides of a dielectric interface in different auxiliary problems are taken equal in magnitude and opposite in direction to ensure the continuity of the tangential components of the fields on these boundaries, as in the original problem. In this procedure the fields produced by the equivalent currents within the region boundaries are the same as those in the original problem, while the zero field is produced outside these boundaries. The electric and magnetic surface currents along the boundaries are

$$\mathbf{J}^i = \hat{\mathbf{n}}_i \times \mathbf{H}^i \quad \text{and} \quad \mathbf{M}^i = -\hat{\mathbf{n}}_i \times \mathbf{E}^i \quad \text{on } S_i \tag{5}$$

Both $\mathbf{J}^i$ and $\mathbf{M}^i$ have components in both the longitudinal, $\hat{\mathbf{z}}$, and transverse, $\hat{\mathbf{t}}_i$, directions, i.e.

$$\begin{Bmatrix} \mathbf{J}^i \\ \mathbf{M}^i \end{Bmatrix} = \begin{Bmatrix} J_z^i \\ M_z^i \end{Bmatrix} \hat{\mathbf{z}} + \begin{Bmatrix} J_t^i \\ M_t^i \end{Bmatrix} \hat{\mathbf{t}}_i, \quad \text{on } S_i \tag{6}$$

where the transverse unit tangent is defined by

$$\hat{\mathbf{t}}_i = \hat{\mathbf{z}} \times \hat{\mathbf{n}}_i \tag{7}$$

where $\hat{\mathbf{n}}_i$ is the unit normal to S_i. The currents on the surface S_i are the sum of the currents on all the boundaries S_{ij}, where $j \neq i$ and j represents all the region numbers adjacent to the region V_i, i.e.

$$\mathbf{J}^i = \sum_{\forall j} J^{ij}, \quad \text{on the boundaries of region } i \tag{8}$$

and similarly for $\mathbf{M}^i$. On the conductor boundaries the magnetic current is zero. We can now obtain the electric and magnetic fields $\mathbf{E}^i(\boldsymbol{\rho}, k_z)$ and $\mathbf{H}^i(\boldsymbol{\rho}, k_z)$ due to the electric current $\mathbf{J}^i(\boldsymbol{\rho}', k_z)$ by using

$$\begin{aligned} \mathbf{E}^i(\boldsymbol{\rho}, k_z) = &- j\omega \mathbf{A}^i(\boldsymbol{\rho}, k_z) \\ &- j\frac{1}{\omega \varepsilon_i \mu_i} \nabla\nabla \cdot \mathbf{A}^i(\boldsymbol{\rho}, k_z) \end{aligned} \tag{9}$$

$$\mathbf{H}^i(\boldsymbol{\rho}, k_z) = \frac{1}{\mu_i} \nabla \times \mathbf{A}^i(\boldsymbol{\rho}, k_z) \tag{10}$$

where the magnetic vector potential $\mathbf{A}$ is

$$\mathbf{A}^i(\boldsymbol{\rho}, k_z) = \frac{\mu_i}{j4} \int_{l'} \mathbf{J}^i(\boldsymbol{\rho}', k_z) H_0^{(2)}(k_\rho \Delta\rho) dl' \tag{11}$$

$$\Delta\rho = |\boldsymbol{\rho} - \boldsymbol{\rho}'|$$

The transverse wave number k_ρ is defined as $k_\rho = \sqrt{k_i^2 - k_z^2}$, $\mathrm{Im}[k_\rho] \leq 0$, where k_i is the wave number in region i. The ∇ operator used here is defined as

$$\nabla = \nabla_t - jk_z\hat{\mathbf{z}} \quad \text{and} \quad \nabla_t = \frac{\partial}{\partial x}\hat{\mathbf{x}} + \frac{\partial}{\partial y}\hat{\mathbf{y}} \tag{12}$$

After some mathematical manipulations the electric and magnetic fields due to the electric currents can be expressed in operator form as shown in [7, Appendix A]. Expressions are given for $E_t^i(J_t^i)$, $E_z^i(J_t^i)$, $E_t^i(J_z^i)$, and $E_z^i(J_z^i)$ which are each of the components of the vector operator $\mathbf{E}_{tan}^i(\mathbf{J}^i)$ for the tangential E-field at a point $\boldsymbol{\rho}$ on S_i, and in the same fashion we get $H_t^i(J_t^i)$, $H_z^i(J_t^i)$, and $H_t^i(J_z^i)$ for the tangential H-field vector operator $\mathbf{H}_{tan}^i(\mathbf{J}^i)$, i.e.

$$\begin{aligned} \mathbf{E}_{tan}^i(\mathbf{J}^i) = &[E_t^i(J_t^i) + E_t^i(J_z^i)]\hat{\mathbf{t}}_i \\ &+ [E_z^i(J_t^i) + E_z^i(J_z^i)]\hat{\mathbf{z}} \end{aligned} \tag{13}$$

$$\mathbf{H}_{tan}^i(\mathbf{J}^i) = [H_t^i(J_t^i) + H_t^i(J_z^i)]\hat{\mathbf{t}}_i + H_z^i(J_t^i)\hat{\mathbf{z}} \tag{14}$$

The fields due to the magnetic current $\mathbf{M}^i(\boldsymbol{\rho}', k_z)$ can be obtained by using duality [8, Ch.3,Sec.3-2]. The

boundary conditions must now be enforced on each boundary of the object. The boundary conditions are:

$$\begin{aligned} &-[\mathbf{E}^i_{tan}(\mathbf{J}^i) + \mathbf{E}^j_{tan}(\mathbf{J}^i) + \\ &\quad \mathbf{E}^i_{tan}(\mathbf{M}^i) + \mathbf{E}^j_{tan}(\mathbf{M}^i)] \\ &= [\mathbf{E}^i_{tan}(\mathbf{J}^{i,inc}) - \mathbf{E}^j_{tan}(\mathbf{J}^{j,inc}) + \\ &\quad \mathbf{E}^i_{tan}(\mathbf{M}^{i,inc}) - \mathbf{E}^j_{tan}(\mathbf{M}^{j,inc})] \quad \text{on } S_{ij} \end{aligned} \tag{15}$$

and

$$\begin{aligned} &-\hat{\mathbf{n}}_i \times [\mathbf{H}^i_{tan}(\mathbf{J}^i) + \mathbf{H}^j_{tan}(\mathbf{J}^i) + \\ &\quad \mathbf{H}^i_{tan}(\mathbf{M}^i) + \mathbf{H}^j_{tan}(\mathbf{M}^i)] \\ &= \hat{\mathbf{n}}_i \times [\mathbf{H}^i_{tan}(\mathbf{J}^{i,inc}) - \mathbf{H}^j_{tan}(\mathbf{J}^{j,inc}) + \\ &\quad \mathbf{H}^i_{tan}(\mathbf{M}^{i,inc}) - \mathbf{H}^j_{tan}(\mathbf{M}^{j,inc})] \\ &\quad \text{on } S_{ij}, \text{ just inside } V_j \end{aligned} \tag{16}$$

If the boundary S_{ij} is a conducting boundary and the region V_j is a conducting region equations (15) and (16) become

$$-\mathbf{E}^i_{tan}(\mathbf{J}^i) = [\mathbf{E}^i_{tan}(\mathbf{J}^{i,inc}) + \mathbf{E}^i_{tan}(\mathbf{M}^{i,inc})] \quad \text{on } S_{ij} \tag{17}$$

and

$$\begin{aligned} &-\hat{\mathbf{n}}_i \times \mathbf{H}^i_{tan}(\mathbf{J}^i) = \\ &\quad \hat{\mathbf{n}}_i \times [\mathbf{H}^i_{tan}(\mathbf{J}^{i,inc}) + \mathbf{H}^i_{tan}(\mathbf{M}^{i,inc})] \\ &\quad \text{on } S_{ij}, \text{ just inside } V_j \end{aligned} \tag{18}$$

Substituting operators for the fields into the expressions for the boundary conditions yields the integral equations. Only one of equations (17) and (18) is needed to solve for the unknown currents. If equation (17) is used on the perfect electric conductor (PEC) with (15) and (16) on the dielectric boundary, the formulation is called the E-PMCHW formulation. If equation (18) is used just inside the PEC boundary with (15) and (16) on the dielectric boundary, the formulation is referred to as H-PMCHW. The C-PMCHW formulation can be obtained if equations (17) and (18) are combined and used as one equation together with (15) and (16), [9]. Following the method of moments, the object contour C is divided into N linear segments with length ΔC^l, $l = 1, 2, ..., N$ as in [9], and each current component is expanded into N pulse basis functions p^l. In equation form, the unknown currents can be expressed as

$$\mathbf{J}^i = \sum_{l=1}^{N} (I_t^{l,i}\hat{\mathbf{t}}_i + I_z^{l,i}\hat{\mathbf{z}})p^l \quad \text{on all } S_{ij} \tag{19}$$

and

$$\mathbf{M}^i = \sum_{l=N+1}^{N+N_d} (M_t^{l,i}\hat{\mathbf{t}}_i + M_z^{l,i}\hat{\mathbf{z}})p^l \quad \begin{matrix}\text{on dielectric} \\ \text{boundaries}\end{matrix} \tag{20}$$

where $I_t^{l,i}$, $I_z^{l,i}$, $M_t^{l,i}$, and $M_z^{l,i}$ are the unknown electric and magnetic current coefficients. The pulse functions is $p^l = 1$ on the subdomain ΔC^l and zero elsewhere. N_d is the number of segments on the dielectric boundaries. Substituting (19) and (20) into the operators defined in [7, Appendix A] and then substitute the operators in (12) to (15) and satisfy (12) to (15) at the match point (middle of the segments), the integral equations reduce to a matrix equation of order $2(N + Nd)$, which can be written in the form of a matrix equation (21).

The elements of these submatrices are given in [7, Appendix B] where $Z^{ij,i}_{\alpha\beta}$ and $Y^{ij,i}_{\alpha\beta}$ denote matrix elements obtained from the operators $E^i_\alpha(J^j_\beta)$ and $H^i_\alpha(J^j_\beta)$, respectively, on the surface S_{ij} from the region i. Therefore, the first suffix of the subscripts refers to the field component and the second suffix of the subscript refers to the current component. The first pair of the superscripts refers to the surface boundary ij and the second suffix of the superscripts refers to the region number i or j. This matrix is built assuming all the boundaries are dielectric boundaries, but on the conductor parts the columns and the rows that are corresponding to the magnetic currents and the magnetic field, respectively, which are in the third and forth columns and rows, respectively, must be removed and in the first and second columns of (21) the parts that are corresponding to conducting regions i or j must be forced to zero.

The quantities I_z^{ij}, I_t^{ij}, M_z^{ij}, and M_t^{ij} are the unknown expansion coefficients of the electric and magnetic currents, respectively. The right side columns are the excitation vectors, where $V_z^{ij,i}$, $V_t^{ij,i}$, $I_z^{ij,i}$, and $I_t^{ij,i}$ denote the incident electric and magnetic fields,

$$\begin{bmatrix} Z^{ij,i}_{zz} + Z^{ij,j}_{zz} & Z^{ij,i}_{zt} + Z^{ij,j}_{zt} & Y^{ij,i}_{zz} + Y^{ij,j}_{zz} & Y^{ij,i}_{zt} + Y^{ij,j}_{zt} \\ Z^{ij,i}_{tz} + Z^{ij,j}_{tz} & Z^{ij,i}_{tt} + Z^{ij,j}_{tt} & Y^{ij,i}_{tz} + Y^{ij,j}_{tz} & Y^{ij,i}_{tt} + Y^{ij,j}_{tt} \\ Y^{ij,i}_{tz} + Y^{ij,j}_{tz} & Y^{ij,i}_{tt} + Y^{ij,j}_{tt} & -\frac{1}{\eta_i}Z^{ij,i}_{tz} - \frac{1}{\eta_j}Z^{ij,j}_{tz} & -\frac{1}{\eta_i}Z^{ij,i}_{tt} - \frac{1}{\eta_j}Z^{ij,j}_{tt} \\ Y^{ij,i}_{zz} + Y^{ij,j}_{zz} & Y^{ij,i}_{zt} + Y^{ij,j}_{zt} & -\frac{1}{\eta_i}Z^{ij,i}_{zz} - \frac{1}{\eta_j}Z^{ij,j}_{zz} & -\frac{1}{\eta_i}Z^{ij,i}_{zt} - \frac{1}{\eta_j}Z^{ij,j}_{zt} \end{bmatrix} \begin{bmatrix} I_z^{ij} \\ I_t^{ij} \\ M_z^{ij} \\ M_t^{ij} \end{bmatrix} = \begin{bmatrix} V_z^{ij,i^{inc}} - V_z^{ij,j^{inc}} \\ V_t^{ij,i^{inc}} - V_t^{ij,j^{inc}} \\ I_z^{ij,i^{inc}} - I_z^{ij,j^{inc}} \\ I_t^{ij,i^{inc}} - I_t^{ij,j^{inc}} \end{bmatrix} \tag{21}$$

respectively, on the surface S_{ij} due to all electric and magnetic sources in region i.

4 Farfields

Once the moment method matrix equation is solved the farfields due to the currents on the outer surface boundary and the current sources in the exterior region can be computed. The field will be along a cone of half angle $\theta = \arccos(k_z/k_0)$ around the structure. The farfield operators for electric and magnetic surface currents in the (ρ, k_z)-domain are given in [1]. Our surface currents are expressed in their local coordinate system $(\hat{n}', \hat{t}', \hat{z})$ and since farfields are most conveniently expressed in a spherical coordinate system, we need to do a coordinate transformation. Using a one-point midpoint rule for the integration, the result is:

$$E_\theta = -j\frac{k}{4\pi}\frac{e^{-jkr}}{r} \left[\eta_0 \sum_{l=1}^{N_0} \left(\tilde{J}_t^{l,0}\frac{k_z}{k}(\hat{t}_l'\cdot\hat{\rho}) - \tilde{J}_z^{l,0}\frac{k_\rho}{k}\right) e^{jk_\rho \vec{\rho}_l'\cdot\hat{\rho}}\Delta C^l + \sum_{l=N_0+1}^{N_0+N_d} \tilde{M}_t^{l,0}(\hat{n}_l'\cdot\hat{\rho}) e^{jk_\rho\vec{\rho}_l'\cdot\hat{\rho}}\Delta C^l\right] \tag{22}$$

$$E_\phi = -j\frac{k}{4\pi}\frac{e^{-jkr}}{r} \left[\eta_0 \sum_{l=1}^{N_0} \tilde{J}_t^{l,0}(\hat{n}_l'\cdot\hat{\rho}) e^{jk_\rho\vec{\rho}_l'\cdot\hat{\rho}}\Delta C^l - \sum_{l=N_0+1}^{N_0+N_d} \left(\tilde{M}_t^{l,0}\frac{k_z}{k}(\hat{t}_l'\cdot\hat{\rho}) + \tilde{M}_z^{l,0}\frac{k_\rho}{k}\right) e^{jk_\rho\vec{\rho}_l'\cdot\hat{\rho}}\Delta C^l\right] \tag{23}$$

5 Results and Discussion

The formulation presented in the previous sections has been implemented in a computer program. We have validated the code against previously published results: radiation from slot antennas [2, 3] and radiation from dipole antennas [4]. The code has also been validated against series solutions for homogeneous dielectric cylinders. In the following subsections we present validation cases involving composite dielectric/PEC structures: we compare our moment method results against a series solution for the scattered field from a dielectric cylinder under oblique plane wave illumination, measured radiation pattern from a slotted waveguide array of tilted slots in a trough partially filled with dielectric material, and calculated patterns for a four-element dipole antenna on a TV-mast covered by a thin radome.

5.1 Verification of Scattering Problems (plane wave excitation)

In order to verify the code, an exact series solution for a dielectric coated circular metal cylinder under oblique plane wave incidence with arbitrary polarization was derived in a similar way as the solution for the dielectric cylinder in [10, Ch.17,pp.144-148], and as extended in [11]. The exact and numerical solutions for the scattering widths are compared with each other in Fig. 3 for a plane wave incident from $\theta_i = 45°$, $\phi_i = 180°$ and $\alpha_i = 45°$, α_i is the angle between the incident electric field and the plane of incidence (the $z-k$ plane). The angles are defined such that the Poynting vector S of the incident wave makes an angle ϕ_i with the x-axis of the scatterer's coordinate system and an angle θ_i with the scatterer's xy-plane, where positive θ angles make the Poynting vector point below the xy-plane. The electric field makes an angle α with the plane spanned by the scatterer's z-axis and the Poynting vector, such that the projection of the electric field on $\hat{z}\times\mathbf{S}$ is positive. The radius of the PEC cylinder is $ka = 1.885$ and the outer is $ka = 3.0$. We use twenty segments per wavelength on all material interfaces, where the wavelength is the wavelength in the material. The largest difference between the two calculations is seen to be about 0.5dB for σ_ϕ around 120°, Fig. 3.

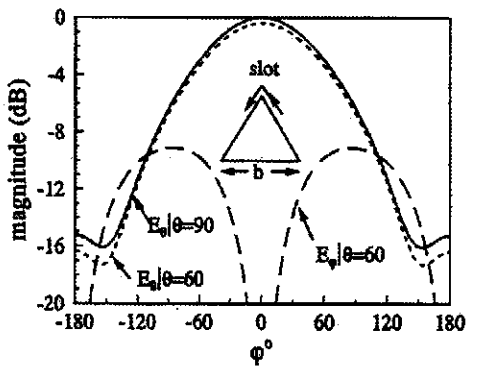

Figure 2: Radiation patterns of an edge slot on a triangular conducting post. $b = 0.4\lambda$. The horizontal pattern ($\theta = 90°$) is indistinguishable from the result in [3]. The dashed curves are predicted farfield components on the cone $\theta = 60°$.

5.2 Slot Excitation (equivalent magnetic current source)

Here we are going to present two different examples. The first example is the radiation from an edge slot on a triangular waveguide for base station antenna

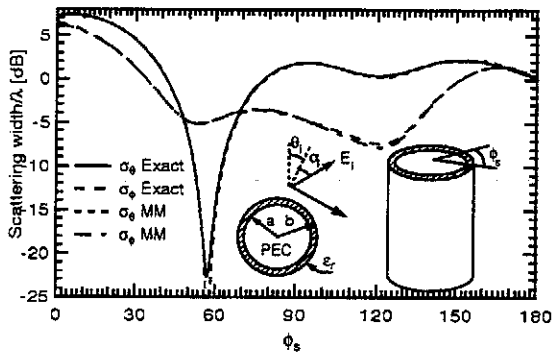

Figure 3: Scattering width from an infinitely long circular cylinder under oblique planewave incidence, $\alpha_i = \pi/4$, $\theta_i = \pi/4$, and $\phi_i = \pi$. The cylinder radii are $ka = 1.885$ and $kb = 3$, The relative dielectric constant is $\epsilon_r = 4$. Exact series solution (solid) and MM solution (dashed) using 20 basis functions per wavelength. The wavelength is taken as the wavelength in the dielectric.

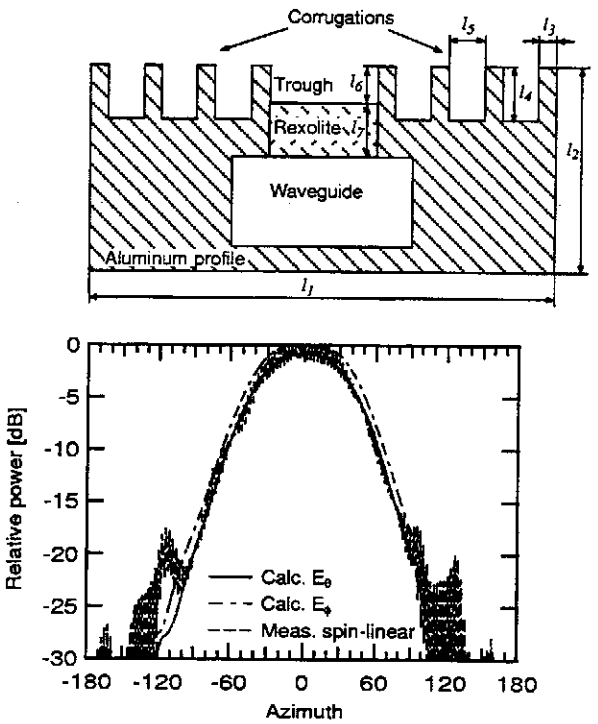

Figure 4: Cross-section of waveguide array designed for circular polarization. $l_1 = 131$mm, $l_2 = 58$, $l_3 = 5$mm, $l_4 = 15$mm, $l_5 = 10$mm, $l_6 = 10$mm, $l_7 = 15$mm, $\epsilon_r = 2.62$. Waveguide $WR187$, $f = 4.9$GHz. The slots are rotated 18.5° with respect to the waveguide axis and radiate into a trough partially filled with dielectric material to achieve circular polarization. The antenna is corrugated outside the trough to control the pattern in azimuth. Measured (solid) and calculated (dashed) show reasonable agreement.

application. The side of the triangle is 0.4λ long. Three slots, one on each edge of the triangle will satisfy the 360° required coverage for this base station. The geometry and the radiation patterns are shown in Fig. 2. Our computed results agrees well with the computed pattern presented in [3] for the horizontal pattern ($\theta = 90°$, i.e. $k_z = 0$). Here, we also present the radiation patterns for the cone cut $\theta = 60°$.

Slot antennas have been extensively used in arrays for radar applications. Normally the slot arrays are exited by a rectangular or parallel plate waveguide. Circular polarization fields of the slot antenna are normally obtained by slot pairs properly oriented to each other with a 90° phase difference between the slot aperture fields. Narrow slot apertures are also used to excite microstrip antennas. For circular polarization two perpendicular slots coupled to two microstrip lines with 90° phase shift are used to produce circular polarization. In Fig. 4 we present a single slot antenna element which radiate circular polarization. The slot is located in the broad wall of a rectangular waveguide and it is loaded by a dielectric slab and surrounded by baffles within a corrugated ground plane. The slot is rotated 18.5° with respect to the centerline of the waveguide to give the proper axial ratio for circular polarization. The thickness of the dielectric loading and the height and width of the trough are designed to provide the required quadratic phase difference between the two field components. The numerical and measured results showed a good promising performance of this element.

5.3 Dipole Excitation (equivalent electric current source)

In this section we verify the dipole part of the computer program to previously published results and an in-house code for concentric multilayer circular cylinders. In Fig. 5 we see a circular PEC rod coated with two concentric layers of dielectric. A Hertz dipole is embedded inside the outer dielectric and tilted 45° to the z-axis. The elevation and azimuth patterns are calculated by both the present MM code and an in-house code for concentric multilayer circular cylinders where the fields are expanded in cylindrical modes [12]. In the MM solution we use 20 basis functions per wavelength and current component on all material interfaces. The wave length is taken as the shortest in the two contiguous media sharing the same boundary, i.e. the three cylindrical interfaces are divided in 64, 76, and 79 segments respectively starting with the PEC cylinder. This gives a total of 876 unknowns.

The difference in azimuth pattern for both polarizations when using only ten segments per wave length was less than 0.19dB.

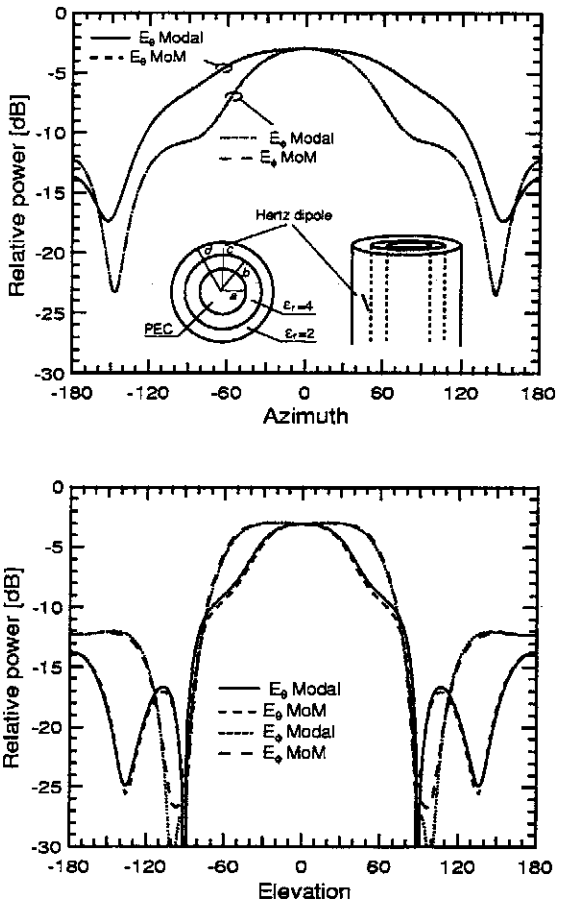

Figure 5: A circular PEC rod coated with two concentric dielectric layers with a 45° tilted electric Hertz dipole in the outer layer. The elevation and azimuth patterns are calculated by the present moment method and compared to a code for coaxial multilayer circular cylinders [12]. $a = 0.25\lambda$, $b = 0.3\lambda$, $c = 0.375\lambda$, $d = 0.45\lambda$

The other verification case consists of four horizontal half wavelength dipoles as shown in the insertion of Fig. refTVmast, one dipole on each side of the square metallic post [13]. We have calculated the horizontal radiation patterns ($k_z = 0$, $\theta = 90°$) with and without a circular cylindrical thin radome enclosing the post and the dipoles, Fig. 6. The horizontal patterns agrees to within the resolutions of the graphs presented in [13]. We have also included our predicted results for an elevation angle of 30° from the horizontal plane ($k_z = 0.5k_0$, $\theta = 60°$).

6 Conclusion

A computer code for analysis of radiation and scattering from 2D structures with 3D sources (and oblique plane wave incidence) has been developed. The 2D structures consists of any number of infinitely long composite cylinders, where each cylinder can have any number of dielectric and PEC regions. The sources we consider here are dipoles and slots that are arbitrarily oriented with respect to the composite cylinder and can be either inside a dielectric region or in the surrounding free space or on the interface between two regions.

The code has been verified in several different ways: analytic series solutions, other numerical results and measured data. In all cases the code performed as expected.

Acknowledgment

We would like to thank Dr. Zvonimir Šipuš for generating the validation curves for the double-layer coaxial cylinder excited by a Hertz dipole.

This work was partially supported by the National Science Foundation under Grant no. ECS-9809862, and by the Swedish National Board for Industrial and Technical Development, NUTEK.

References

[1] P.-S. Kildal, S. Rengarajan, and A. Moldsvor, "Analysis of nearly cylindrical antennas and scattering problems using a spectrum of two-dimensional solutions," *IEEE Trans. Antennas and Propagat.*, vol. 44, pp. 1183–1192, Aug. 1996.

[2] K. Forooraghi and P.-S. Kildal, "Transverse radiation pattern of a slotted waveguide array radiating between finite height baffles in terms of a spectrum of two-dimensional solutions," *IEE Proceedings-H*, vol. 140, pp. 52–58, 1993.

[3] J. Hirokawa, J. Wettergren, P.-S. Kildal, M. Ando, and N. Goto, "Calculation of external aperture admittance and radiation pattern of a narrow slot cut across an edge of a sectoral cylinder in terms of a spectrum of two-dimensional solutions," *IEEE Trans. Antennas and Propagat.*, vol. 42, pp. 1243–1249, 1994.

[4] P. Slättman, J. Wettergren, and P.-S. Kildal, "Three-dimensional radiation from dipoles in the

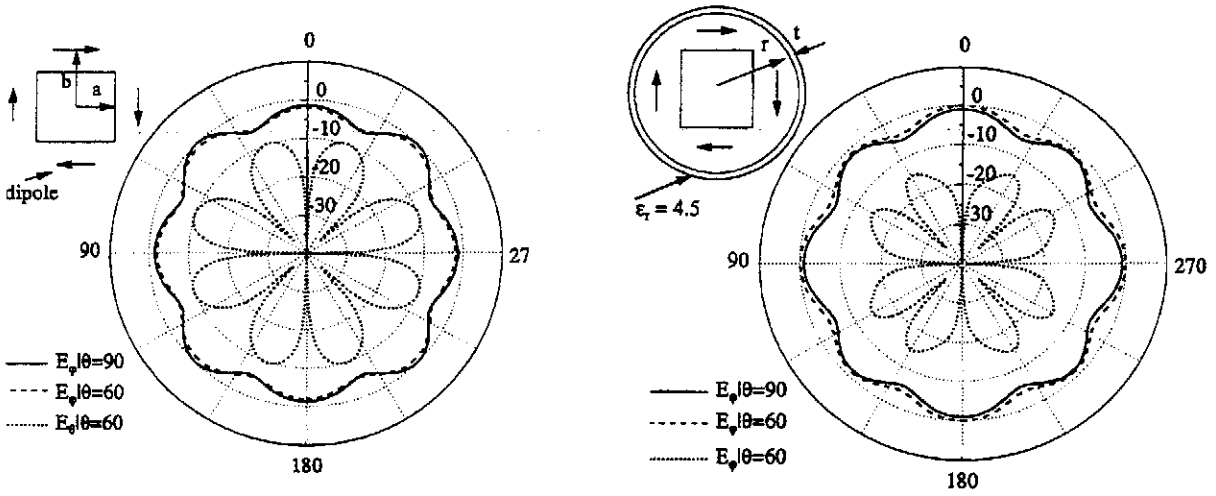

Figure 6: Radiation pattern of four dipoles around a square conducting post with $a = 35$cm, $b = 47.5$cm and $f = 600$MHz (*left*). The same antenna surrounded by a thin dielectric radome with $r = 70$cm and $t = 1.5$cm (*right*).

presence of a conducting strip," in *IEEE AP-S Symp.*, pp. 2266–2269, June 1994.

[5] J. Wettergren and P. Slättman, "An electric field integral equation for cylindrical structures," *IEE Proceedings-H*, vol. 143, pp. 147–151, April 1996.

[6] A. A. Kishk and P. M. Goggans, "Electromagnetic scattering from two-dimensional composite objects," *Applied Computational Electromagnetic Society Journal*, vol. 9, pp. 32–39, 1994.

[7] A. A. Kishk and P.-S. Kildal, "Electromagnetic scattering from two dimensional anisotropic impedance objects under oblique plane wave incidence," *ACES Journal*, vol. 10, no. 3, pp. 81–92, 1995.

[8] R. F. Harrington, *Time Harmonic Electromagnetic Fields*. McGraw-Hill, 1961.

[9] A. A. Kishk and L. Shafai, "Different formulations for numerical solutions of single or multibodies of revolution," *IEEE Trans. Antennas and Propagat.*, vol. AP-34, pp. 666–673, 1986.

[10] J. R. Wait, *Electromagnetic Radiation from Cylindrical Structures*. Peter Peregrinus Ltd., reprint ed., 1988.

[11] A. A. Kishk and P.-S. Kildal, "Asymptotic boundary conditions for strip loaded scatterers applied to circular dielectric cylinders under oblique incidence," *IEEE Trans. Antennas and Propagat.*, vol. 45, pp. 51–56, Jan. 1997.

[12] Z. Šipuš, P.-S. Kildal, R. Leijon, and M. Johansson, "An algorithm for calculating Green's functions for planar, circular cylindrical and spherical multilayer substrates." Accepted for publication in *ACES Journal*.

[13] A. Sadigh and E. Arvas, "Deformation of the horizontal radiation pattern of TV transmitting antennas due to a thin dielectric radome," *IEEE Trans. Antennas and Propagat.*, vol. 40, pp. 942–949, 1992.